Thermodynamic properties at the Earth's core conditions and the shock-reduced isotherm of iron: a first-principles study

2002 J. Phys.: Condens. Matter 14 7321

(http://iopscience.iop.org/0953-8984/14/31/304)

INSTITUTE OF PHYSICS PUBLISHING JOURNAL OF PHYSICS: CONDENSED MATTER

J. Phys.: Condens. Matter **14** (2002) 7321–7335 PII: S0953-8984(02)38040-8

Thermodynamic properties at the Earth's core conditions and the shock-reduced isotherm of iron: a first-principles study

Y Wang[1,2], **R Ahuja**[1] **and B Johansson**[1,3]

[1] Condensed Matter Theory Group, Department of Physics, Uppsala University, Box 530, S-751 21, Uppsala, Sweden
[2] Institute of Applied Physics and Computational Mathematics, PO Box 8009, Beijing, 100088, People's Republic of China
[3] Applied Materials Physics, Department of Materials Science and Engineering, Royal Institute of Technology, S-100 44, Stockholm, Sweden

Received 12 June 2002
Published 24 July 2002
Online at stacks.iop.org/JPhysCM/14/7321

Abstract

First-principles thermodynamic calculations for metal iron (Fe) at ultrahigh pressures and temperatures are reported. The calculated results can be divided into three major parts: (i) the static 300 K equation of state and the dynamic shock-wave Hugoniot at pressures up to 1000 GPa; (ii) the shock-reduced data for the 300 K isotherm; and (iii) the thermodynamic properties under the Earth's core conditions. The calculations are parameter free in the sense that the cold part of the Helmholtz free energy is calculated using the full-potential linearized augmented-plane-wave method within the generalized gradient approximation. The thermal part due to the lattice ions is calculated using the recently developed classical mean-field potential approach, and the thermal part due to the thermal electrons is calculated using the one-dimensional numerical integration technique. The calculated results agree well with the available experimental data.

1. Introduction

In recent years, studies of iron (Fe) have received a lot of attention in the fields of high-pressure physics and basic science—including static diamond-anvil-cell (DAC) experiments [1–6], dynamic shock-wave experiments [7–14], laser-driven shock-wave experiments [15], and *ab initio* simulations [16–23]. The main cause for this interest is Fe being the predominant element of the Earth's core [24]. In order to carry out an accurate hydrodynamic calculation of the evolutionary and dynamic processes within the core, well-constrained thermodynamic parameters of Fe under conditions of high temperatures and high pressures are crucial.

The present work reports systematic first-principles thermodynamic calculations on Fe over a temperature range of 300–30 000 K and a pressure range of 0–1000 GPa using the

recently developed classical mean-field potential (MFP) approach [25, 26] in conjunction with the full-potential linearized augmented-plane-wave method (LAPW) [27]. The motivation behind the present work is threefold:

(i) Experimentally, the physics of condensed matter at ultrahigh pressures can be investigated in both static DAC experiments and dynamic shock-wave experiments. The low-temperature DAC technique is suitable for the ordinary laboratory in which samples can be studied under controlled environment conditions, and recent progress [3, 5] has extended the pressure range for accurate lattice parameter determinations to over 300 GPa. In contrast, shock-wave methods [9, 10, 12] can reach higher-temperature and higher-pressure conditions, but the measurement of the temperature is difficult in comparison with the DAC method. As a result of the tremendous technical advances in recent years, the two techniques have been brought into close contact with each other, and it is highly desirable to theoretically compare and evaluate the measurements made by the two techniques, as well as to build a theoretical bridge between them.

(ii) As already mentioned, the thermodynamic parameters of the Earth's core are of considerable geophysical interest. The seismological data from the preliminary reference Earth model (PREM) [24] suggest that the core, in the depth from 2891 to 6371 km, is composed of mainly Fe and to some extent other, light elements. Therefore, a good description of the Earth's core is dependent, to first order, on the careful constraining of the thermodynamic properties of Fe.

(iii) In a couple of papers [25, 26], we developed the MFP approach to calculate the various kinds of thermodynamic quantity for a metal. With the well-known Dugdale and MacDonald [28] expression for the Grüneisen constant explicitly deduced, the MFP has been tested on the metal Ce, indicating that the well-known γ–α isostructural transition, the experimental Hugoniot data, and the 300 K static equation of state (EOS) were well reproduced [25]. The MFP approach has also been evaluated for five reference metals: Al, Cu, Ta, Mo, and W, indicating that both the calculated Hugoniots and the 293 K isotherms agree well with the experimental data [26]. These promising results have encouraged us to study wide ranges of thermodynamic properties of Fe as a more serious test of the MFP approach.

The rest of this work is organized as follows. In section 2 we briefly introduce the MFP approach. The calculational details and 0 K results are summarized in section 3. Section 4 presents the calculated 300 K static EOS and the calculated Hugoniot states. Section 5 reports our reduced shock-wave data. In section 6 we consider the thermodynamic parameters under the Earth's core conditions. Finally, section 7 contains our conclusions.

2. Thermodynamic model

It is customary to consider the Helmholtz free energy $F(V, T)$ per ion of a substance as consisting of additive static, ionic, and thermal electronic excitation contributions [29], i.e. for a given crystal structure at the given atomic volume V and temperature T we write

$$F(V, T) = E_c(V) + F_{ion}(V, T) + F_{el}(V, T), \tag{1}$$

where $E(V)$ is the 0 K total energy per ion, $F_{ion}(V, T)$ is the vibrational free energy of the lattice, and $F_{el}(V, T)$ includes the free energy due to thermal excitation of electrons from their ground state and also contains the magnetic contribution.

Following the previous work [25, 26, 30], F_{ion} is given by

$$F_{ion}(V, T) = -k_B T \left[\frac{3}{2} \ln \frac{m k_B T}{2\pi\hbar^2} + \ln v_f(V, T) \right], \tag{2}$$

where

$$v_f(V,T) = 4\pi \int \exp\left(-\frac{g(r,V)}{k_B T}\right) r^2 \,\mathrm{d}r. \tag{3}$$

The MFP [25, 26] $g(r, V)$ has simply been constructed in terms of the 0 K total energy $E_c(R)$ as follows:

$$g(r,V) = \tfrac{1}{2}[E_c(R+r) + E_c(R-r) - 2E_c(R)], \tag{4}$$

where r represents the distance that the lattice ion deviates from its equilibrium position R and where V is the atomic volume with respect to R.

One might doubt whether equation (4) will work for lower-symmetry systems such as hcp Fe [31]. In fact, different choices of the coordinate system (such as the Wigner–Seitz radii or the lattice constant) only introduce a structural constant into v_f in equation (3), and this also means a structural constant in the entropy. We note that this structural constant will be automatically removed since almost all measurable thermodynamic quantities only involve differentials of v_f in some form.

From equation (2), the thermal energy due to the lattice ion is

$$E_{ion}(V,T) = k_B T \xi(T,V), \tag{5}$$

with

$$\xi(V,T) = \frac{3}{2} + \left[\frac{\partial \ln v_f(V,T)}{\partial \ln T}\right]_V. \tag{6}$$

Using this function $\xi(T, V)$, the specific heat due to the lattice ion at constant volume is then given by

$$C_V^{ion}(V,T) = k_B\left\{\xi(V,T) + T\left[\frac{\partial \xi(V,T)}{\partial T}\right]_V\right\}. \tag{7}$$

When the magnetic contribution and the electron–phonon interactions are neglected, the electronic contribution to the free energy is given by $F_{el} = E_{el} - TS_{el}$, where the bare electronic entropy S_{el} takes the form [17, 32]

$$S_{el}(V,T) = -k_B \int n[f \ln f + (1-f)\ln(1-f)]\,\mathrm{d}\epsilon, \tag{8}$$

and where n is the electronic density of states (DOS) and f is the Fermi distribution function. With respect to equation (8), the energy E_{el} due to thermal excitations of electrons from their ground state can be expressed as [33]

$$E_{el}(V,T) = \int nf\epsilon \,\mathrm{d}\epsilon - \int^{\epsilon_F} n\epsilon \,\mathrm{d}\epsilon, \tag{9}$$

where ϵ_F is the Fermi energy.

Through equations (5) and (9), the total internal energy can be expressed by

$$E(V,T) = E_{ion}(V,T) + E_{el}(V,T) \tag{10}$$

and the total constant-volume heat capacity is given by

$$C_V(V,T) = C_V^{ion}(V,T) + \left[\frac{\partial E_{el}(V,T)}{\partial T}_V\right]. \tag{11}$$

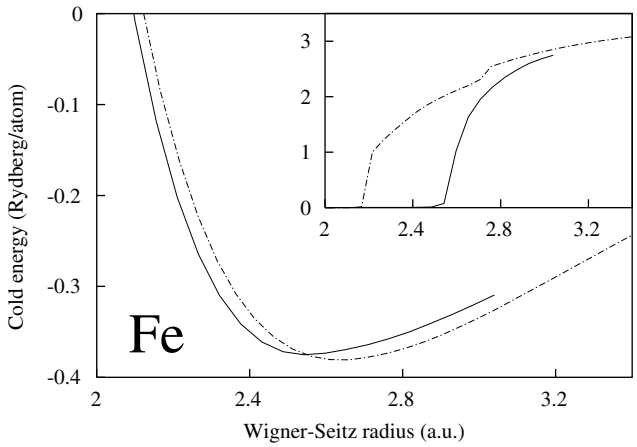

Figure 1. The calculated 0 K total energies and spin magnetic moments per atom as a function of the Wigner–Seitz radius for bcc Fe (dot–dashed curve) and hcp Fe (solid curve).

3. Calculational details and 0 K results

In order to calculate the 0 K total energies, we employ the self-consistent, relativistic (neglecting spin–orbit coupling), full-potential, and spin-polarized LAPW method [27] within the generalized gradient approximation [34]. The basis sets include the semicore 3s and 3p, and the valence 3d, 4s, and 4p partial waves. For the sake of numerical continuity of the calculated energy versus volume relations, we use constant muffin-tin radii (R_{mt}) of 1.75 au for both the bcc (assuming ferromagnetic) structure and the ideal hcp (assuming antiferromagnetic) structure. The plane-wave cut-off K_{cut} is determined by $R_{mt}K_{cut} = 9.0$. 4096 k-points in the full zone are used for reciprocal-space integrations. The calculations are performed for atomic volumes ranging from 100% expansion down to where the muffin-tin spheres touch. The ideal c/a ratio 1.633 is used.

All the thermodynamic parameters are calculated by means of one-dimensional numerical integrations or derivatives. The LAPW calculated 0 K total-energy points are directly taken as input. Outside the range of the LAPW calculation, the cold total energy is obtained by extrapolation using the Morse function.

The 0 K results for the usual bcc and hcp phases have already been discussed elsewhere, including those [16–18] obtained using the LAPW method, those [19] obtained using the LMTO (linear muffin-tin orbital) method, and those [20] obtained using the PAW (projector augmented-wave) method. Our calculated 0 K total energies and spin magnetic moments per atom as functions of the Wigner–Seitz radius for bcc Fe and hcp Fe are depicted in figure 1. In fact, our 0 K properties are very similar to those from the previous calculations done by colleagues. Since the present interest is focused on the finite-temperature case, we will not discuss the 0 K results further in this work.

4. Equation of state

4.1. The bcc–hcp phase transition pressure

Under compression, Fe undergoes a phase transition [35] from the bcc structure to the hcp structure. In general, this transition is centred at 13.0 GPa, is very sluggish, and has a large

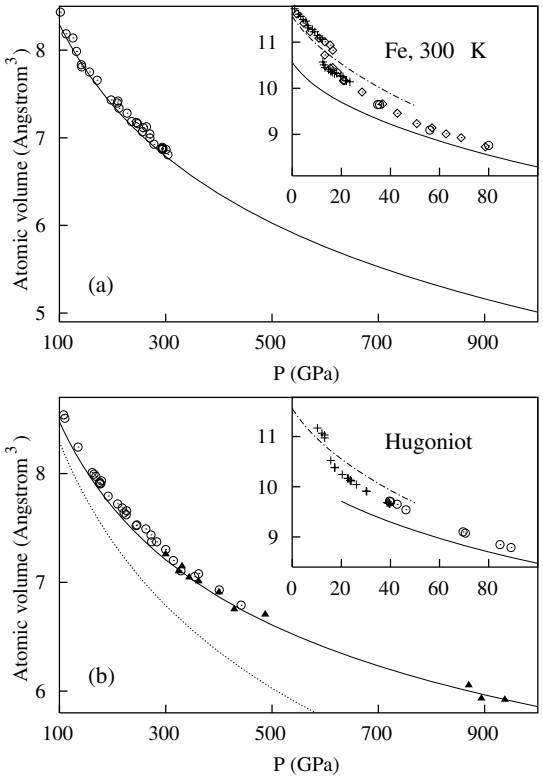

Figure 2. (a) The EOS of the Fe 300 K isotherm. Dot–dashed curve: calculation with the bcc crystal; solid curve: calculation with the hcp crystal; plus signs: DAC data of Huang *et al* [1]; diamonds: DAC data of Jephcoat *et al* [2]; open circles: DAC data of Mao *et al* [3]. (b) The Hugoniot. Dot–dashed curve: calculation with the bcc crystal; solid curve: calculation with the hcp crystal; plus signs: from Barker and Hollenbach [7]; open circles: from Brown *et al* [11]; filled triangles: from Anderson and Ahrens [12]; dotted curve: the calculated 300 K static EOS.

hysteresis. In comparison, our 300 K transition pressure is 14.2 GPa, calculated by equating the Gibbs free energies of the two phases.

4.2. 300 K EOS

The calculated 300 K static EOSs for bcc and hcp Fe are compared with some typical experimental data [1–3] in figure 2(a). For the lower-pressure bcc phase, our calculated results are uniformly lower than the experimental data by ∼2%, which is exactly the same as the deviation between the calculated 300 K equilibrium atomic volume of 11.56 Å^3 and the experimental one [3] of 11.78 Å^3 (7.093 cm^3 mol^{-1}). For the higher-pressure hcp phase, at pressures greater than 70 GPa the comparison between the calculation and the experiment is very similar to the lower-pressure bcc case in the sense that the calculated curve is uniformly lower than the experimental data by a constant value.

The poorest case is that for the lower-pressure region of the hcp phase. When the pressure decreases from 70 GPa, the disagreement between the calculation and the experiment gradually becomes larger. This is a common situation in previous first-principles calculations [16, 19, 20] for Fe. However, since the major interest of the present work is in the higher-compression region, this discrepancy can be circumvented.

4.3. Hugoniot locus

The shock-wave technique [8] is one of the major experimental tools used to explore the various kinds of thermodynamic parameters at ultrahigh pressures. The derived Hugoniot states are characterized by using measurements of the shock velocity (D) and particle velocity (u) with $V_H/V_0 = (D-u)/D$ and $P_H = \rho_0 Du$ where P_H is the pressure and ρ_0 is the initial density. Through the Rankine–Hugoniot relations, these data define a compression curve (volume (V_H) versus pressure (P_H)) as a function of known Hugoniot energy (E_H):

$$\tfrac{1}{2}P_H(V_0 - V_H) = E_H - E_0, \tag{12}$$

where V_0 and E_0 refer to the atomic volume and energy at ambient conditions respectively.

Using the calculated V_0 and E_0 of the bcc structure and numerically solving equation (12), our calculated curves of Hugoniot pressure against volume for bcc and hcp iron are compared with the experimental data [7, 11, 12] in figure 2(b). One can immediately see that the comparisons between the calculations and the experiments are almost a direct copy of the static case. We also plot the calculated 300 K EOS in figure 2(b) using a dotted curve, as an guide to the eye, to demonstrate the large thermal contribution in the Hugoniot with respect to the static 300 K case. Note that, at 1000 GPa, the thermal pressure in the Hugoniot is almost equal to the cold pressure.

Among the very extensive studies on the thermal properties of Fe using the tight-binding total-energy (TBTE) classical cell model, that of Wasserman *et al* [17] also calculated the Fe Hugoniot up to 400 GPa for the hcp phase. The agreement between our MFP result and theirs is very good, while the MFP method considerably simplifies the calculation and can easily be employed even beyond 1000 GPa.

4.4. Heat capacities along the Hugoniot

The constraint of the heat capacities is significant due to the need for measuring the temperatures along the Hugoniot. Our calculated heat capacities along the principal Hugoniot with the hcp structure are presented in figure 3. Since all the thermodynamic quantities reported in this work are calculated by the one-dimensional numerical technique, our calculated heat capacities should be, to date, the most accurate ones in the *ab initio* regime. Note that the thermal electronic contribution to the heat capacity has become non-negligible even at a pressure of 100 GPa; in the region from 160 to 340 GPa, within which Yoo *et al* [13] had measured the Hugoniot temperatures, our calculated constant-volume heat capacity increased from $\sim$35 to $\sim$43 J mol^{-1} K^{-1}.

4.5. Temperature along the Hugoniot

Our predicted temperatures along the principal Hugoniot of Fe in the hcp structure are shown in figure 4 together with the measured data [13, 14]. Note that at the highest pressure of 1000 GPa, the calculated Hugoniot temperature reaches $\sim$30 000 K. The predicted shock-wave temperatures derived from the thermodynamic calculations by Brown and McQueen [9] are also shown for comparison. The agreement between our calculations, those of Brown and McQueen, and the recent experimental data of Ahrens *et al* [14] are excellent. The deviations between our calculation and the experimental results of Yoo *et al* [13] (notice the huge difficulties in the experiment) might due to the constant-volume specific heat of $3k_B$ (24.9 J mol^{-1}) for high-temperature Fe used by Yoo *et al* being somewhat small (see figure 3 for the heat capacity).

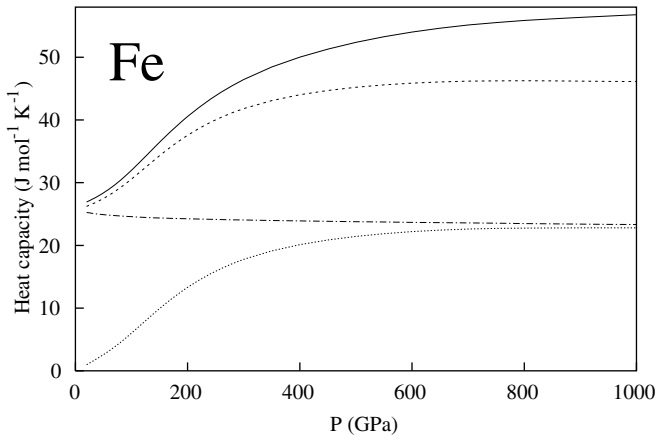

Figure 3. The calculated heat capacities along the principal Hugoniot of hcp Fe. The solid, dashed, dot–dashed, and dotted curves represent the calculated constant-pressure specific heat C_P, constant-volume specific heat C_V, lattice-ion-only constant-volume specific heat C_V^{ion}, and electron-only constant-volume specific heat C_V^{el}, respectively.

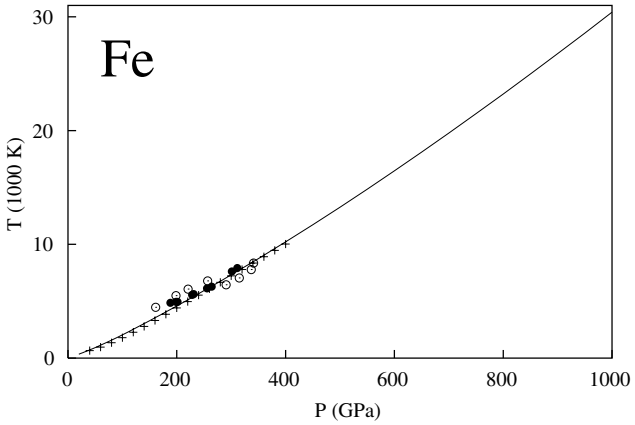

Figure 4. The calculated temperature along the principal Hugoniot of hcp Fe. The solid curve represents the present calculation, the open circles the measured data of Yoo *et al* [13], the solid circles the recent measurements by Ahrens *et al* [14], and the plus signs the thermodynamic analysis of Brown and McQueen [9].

At the shock-wave melting point at 243 GPa, the temperature recently measured by Ahrens *et al* [14] is 5800 K. Our calculated temperature is 5739 K, which is exactly the same value as Laio *et al* [22] calculated using the molecular dynamics (MD) method, is in excellent agreement with the MD calculation by Belonoshko *et al* [23], and falls well within the range of 5700 ± 500 K suggested by Ross *et al* [36].

4.6. Isentropic bulk modulus along the principal Hugoniot

In figure 5 we show our calculated isentropic bulk moduli $B_S(=B_T C_P/C_V)$ along the principal Hugoniot of hcp Fe together with the measured data ($=\rho C^2$, where ρ is the density and C is the sound velocity) for liquid Fe given by Brown and McQueen [9]. Again, our calculated results are very good in comparison with experiment.

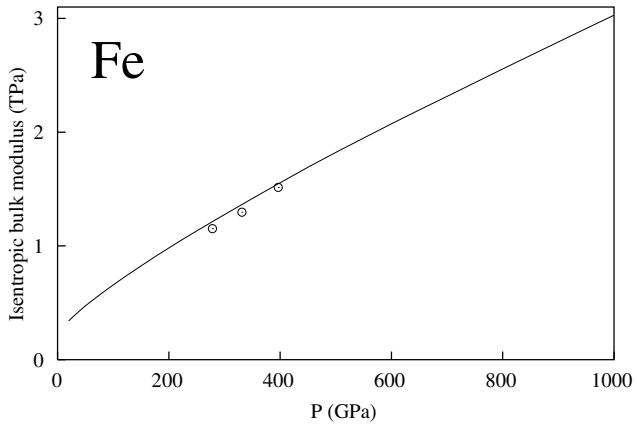

Figure 5. The calculated (solid curve) isentropic bulk moduli along the principal Hugoniot for hcp Fe together with the measured values (open circles) of Brown and McQueen [9].

5. Shock-wave data reduction

In analysing and interpreting both DAC and shock-wave EOS experiments, an important distinction needs to be made between relative and absolute measurements. In the static DAC experiments, only volume is measured from the x-ray line positions whereas the pressure is indirectly inferred from the diffraction line shifts of a pressure marker or reference material, which is mixed with the sample and whose P–V curve is well known. In the dynamic shock-wave experiments, the P–V curve can be deduced directly from the measured data. In fact, almost all the EOS standards used for the DAC measurements are directly or indirectly derived from the reduction of the shock-wave data.

Also, traditionally, the reduction of shock data to isothermal or isentropic states requires specific heat and Grüneisen parameter (γ) values that are not well known. In the absence of experimental constraints, researchers often make plausible speculations [9, 37], such as $\gamma/V =$ constant. Although in the framework of the present MFP approach, both parameters become computable, we have found a very simple scheme which makes no use of these two parameters for the reduction of the shock-wave data.

The great similarity in the comparison between calculations and experiments between the 300 K EOS and the Hugoniot is a demonstration of the accuracy of the MFP approach in calculating the thermal contribution. Therefore, *we simply subtract the thermal volume expansion of the Hugoniot relative to the static 300 K one, calculated by the MFP approach, from the quadratic fitting* [10, 12] *to the shock-wave data*.

5.1. Relative thermal contribution of the Hugoniot to the 300 K case

We first examine the accuracy of the MFP approach in calculating the thermal part in the EOS. The calculated relative thermal contributions of the Hugoniot to the 300 K case are shown in figure 6. Using the fittings to the static and dynamic experimental data, respectively, of Mao *et al* (using the Birch–Murnaghan EOS) [3] and Hixson and Fritz (using a quadratic fitting of the D–u relation) [10], we can derive experimentally based data, and these data are also plotted in figure 6. We find a surprisingly good agreement between the calculation and the experiment—especially so if we consider the errors due to the fittings in both the D–u relation and the DAC data.

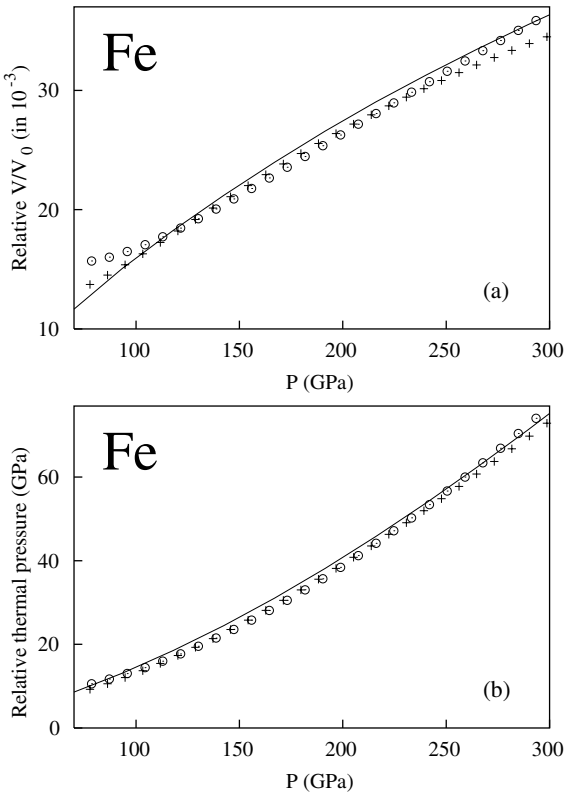

Figure 6. The relative thermal contribution of the Hugoniot to the static 300 K case. Solid curves: the present calculation; plus signs: data deduced by subtracting the 300 K data of Mao *et al* (see [3]; Birch–Murnaghan EOS) from the Hugoniot data of Hixson and Fritz (see [10]; quadratic fitting of the D–u relation); circles: data deduced by subtracting the 300 K data of Mao *et al* [3] from the Hugoniot data of Brown and McQueen (see [9]; quadratic fitting of the D–u relation). (a) Thermal volume expansion of the Hugoniot relative to the 300 K case. (b) Thermal pressure of the Hugoniot relative to the 300 K case.

5.2. Reduced 300 K static EOS

In order to obtain a high accuracy in the reduction of the measured data, we must use an analytical expression for the shock-wave data. Accordingly, we use the quadratic fitted result of Hixson and Fritz [10] for $u \leqslant 5.2$ km s^{-1} and the quadratic fitted result of Anderson and Ahrens [12] for $u \geqslant 5.2$ km s^{-1}.

The numerical results of our reduction are compared with the measured data as well as the fitting using the Birch–Murnaghan EOS and the universal EOS by Mao *et al* [38] in figure 7(a). At pressures less than 300 GPa, our data are almost indistinguishable from those of Mao *et al*. For pressures greater than 300 GPa, our data gradually become softer than the fittings by Mao *et al*.

For convenience, our reduced data have also been fitted with both the original universal EOS of Vinet *et al* [38] and the generalized universal EOS of Moriarty [39]:

$$P_{300}^{rd}(X) = 3B_0[(1-X^{1/3})/X^{2/3}]\exp[\eta(1-X^{1/3}) + \beta(1-X^{1/3})^2 + \xi(1-X^{1/3})^3 + \delta(1-X^{1/3})^4], \tag{13}$$

where $X = V/V_{02}$ with $V_{02} = 11.18$ Å^3 (6.73 cm^3 mol^{-1} from Mao *et al* [3]), η, β, ξ, and δ are fitting parameters, and B_0 represents the equilibrium isothermal bulk modulus. In the case

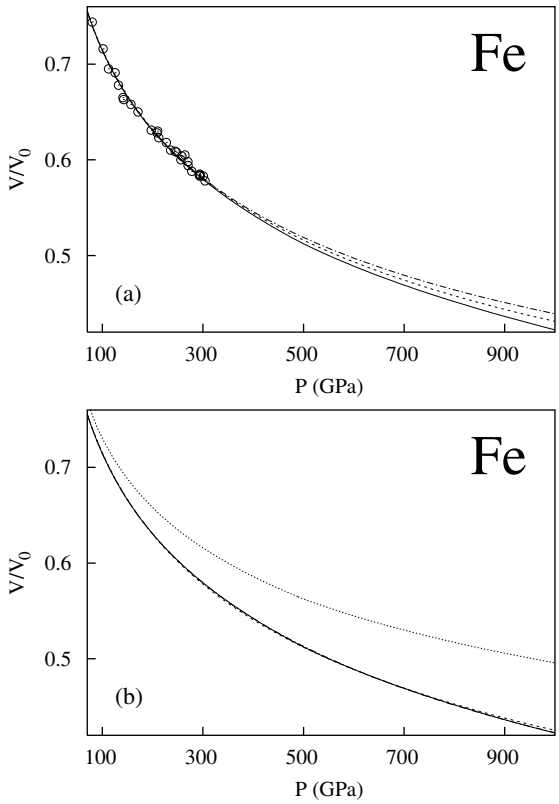

Figure 7. The 300 K static EOS for hcp Fe. (a) Comparison with the experimental data. Solid curve: numerical results from the present reduction; open circles: DAC data of Mao *et al* [3]; dot–dashed curve: Birch–Murnaghan EOS fitting of Mao *et al*; dashed curve: universal EOS fitting of Mao *et al*. (b) Our fittings to the present reduced data. Dashed curve: the universal EOS [38] fitting; dot–dashed curve (overlapping with the solid curve): the generalized universal EOS [39] fitting; dotted curve: the shock-wave data used.

Table 1. The EOS parameters in equation (13) for the present shock-reduced 300 K isotherm of hcp Fe.

EOS	B_0	η	β	ξ	δ
Vinet	165.75	6.8717	0	0	0
Moriarty	207.27	0	71.069	−294.20	414.83

where β, ξ, and δ are all equal to zero, equation (13) reduces to the original universal EOS with $\eta = \frac{3}{2}(B_0' - 1)$, where B_0' represents the pressure derivative of B_0.

The fitted results for B_0, η, β, ξ, and δ are listed in table 1. Figure 7(b) shows the plots of the comparisons between the different fittings and the numerical results. The generalized universal EOS can give a better expression for the numerical data than the original universal EOS. We also plot in figure 7(b) the shock-wave data used for the reduction, by means of a dotted curve as a guide for the eye, to demonstrate the thermal contribution in the Hugoniot curve with respect to the static 300 K curve.

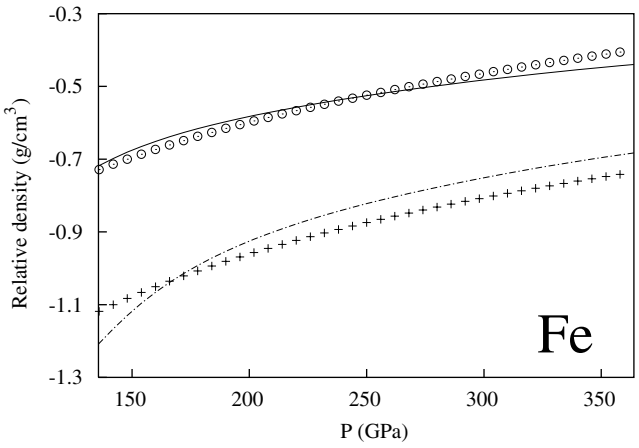

Figure 8. The difference of the high-temperature density and the 300 K density. Solid curve: the present calculation for 5000 K; open circles: deduced by subtracting the 300 K data of Mao *et al* (see [3]; Birch–Murnaghan EOS) from the extrapolated 5000 K data of Dubrovinsky [5]; dot–dashed curve: the present calculation for 7000 K; plus signs: deduced by subtracting the 300 K data of Mao *et al* (see [3]; Birch–Murnaghan EOS) from the extrapolated 7000 K data of Dubrovinsky.

6. Thermodynamic properties relevant to the Earth's core

The thermodynamic properties of Fe under the conditions of the Earth's core pressure ranges [24] of from 135.7 to 363.9 GPa are undoubtedly of utmost importance for the understanding of the behaviour of the core, typically including the convective dynamics and heat transport.

At present, the direct calculation of some thermodynamic parameters, such as the density, is still not sufficiently advanced to reach the desired accuracy. On one hand, an accuracy of 1% in the lattice constant produced by the first-principles calculation could be thought to be excellent; however, it will result in an error of 3% in the density. On the other hand, the Earth's core is not constituted of pure iron. In view of this, it is better to start from a study of relative quantities.

6.1. Densities at 5000 and 7000 K relative to that at 300 K

As the first step, we check our procedure by calculating the density differences at high temperatures relative to those at 300 K. In a very recent letter, Dubrovinsky *et al* [5] have measured the Fe EOS at pressures and temperatures up to 300 GPa and 1300 K. Using these data, they have also extrapolated a 5000 isotherm and a 7000 K isotherm. Using these two isotherms and the 300 K data of Mao *et al* [3], we can deduce two sets of relative densities. Accordingly, we can also derive two sets of equivalent quantities by the MFP approach. These results are compared with each other in figure 8.

Our calculated differences between the 5000 and 7000 K density decrease with increasing pressure (the density difference at 364 GPa is only half that at 136 GPa, whereas the result obtained by Dubrovinsky *et al* is almost unchanged). Nevertheless, we can assume that the agreement is good between these data, considering the error bars of the different model EOS fittings to the experimental data and the 5000 and 7000 K data of Dubrovinsky *et al* being extrapolations.

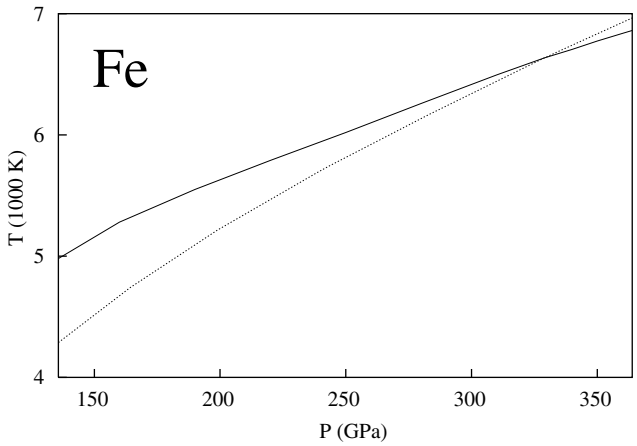

Figure 9. The calculated temperature profile for hcp Fe under the Earth's core conditions (solid curve). The dotted curve represents the calculated high-pressure melting curve of pure hcp Fe [40].

6.2. Temperature profile of the core

In a previous paper [40], we briefly reported the calculated melting temperature of 6635 K for Fe at the outer–inner-core boundary pressure of 328.9 GPa. This melting temperature is, in fact, exactly the same as that derived by the MD method [22].

Having examined the ability of the MFP approach to reproduce the density differences and having derived the melting temperature at the outer–inner-core boundary, we can turn to calculating the temperature profile of the core.

Taking the density, at 328.9 GPa, of the PREM data as the reference point, we can deduce a set of density differences from the PREM data. Subsequently, by reproducing these data theoretically (at a given pressure, changing the temperature, calculating the density, and comparing with the density calculated at 328.9 GPa and 6635 K), we can then derive a set of temperatures under the conditions of the Earth's core. The results are depicted in figure 9. Specifically, at the core–mantle boundary pressure of 135.7 GPa, our calculated temperature is ∼4980 K, and at the core centre, our calculated temperature is ∼6850 K.

6.3. Specific heat under the Earth's core conditions

For reference we have also calculated the specific heat with respect to our calculated temperature profile of the Earth's core, and the results are shown in figure 10. Notice that the calculated constant-volume heat capacities are almost constant, with a value of 40 J mol^{-1} K^{-1}. This is considerably greater than the value of 24.9 J mol^{-1} K^{-1}($3k_B$) obtained by the Dulong–Petit approximation. This large difference is mainly due to the large contribution from the thermal excitation of the electrons.

6.4. Grüneisen parameter under the Earth's core conditions

The thermodynamic Grüneisen parameter γ_{th} can be calculated from

$$\gamma_{th}(V,T) = \frac{V B_T(V,T)\beta_P(V,T)}{C_V(V,T)}, \tag{14}$$

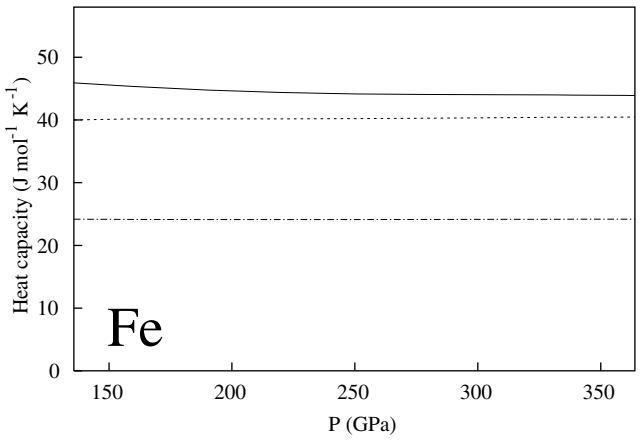

Figure 10. The calculated heat capacities for hcp Fe under the Earth's core conditions. For the key of the curves, see figure 3.

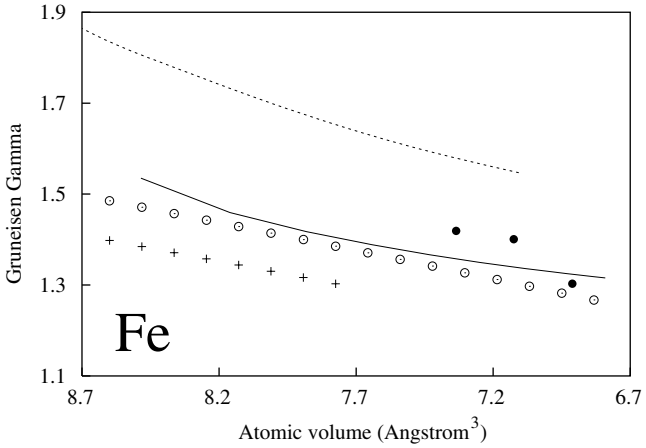

Figure 11. The thermodynamic Grüneisen parameter for hcp Fe. Solid curve: the present calculation; open circles: from Dubrovinsky [5]; plus signs: from Merkel *et al* [4]; solid circles: from Anderson and Ahrens [12]; dashed curve: values calculated by Wasserman *et al* [17].

where B_T is the isothermal bulk modulus and β_P the volume thermal expansion coefficient. In figure 11 we plot our calculated γ_{th} at the Earth's core conditions together with the very recent experimentally based values of Merkel *et al* [4] from Raman spectroscopy [$\gamma = 1.68(V/V_{02})^{0.7}$], of Dubrovinsky *et al* [5] from the DAC [$\gamma = 1.78(V/V_{02})^{0.69}$], and of Anderson and Ahrens [12] from shock-wave studies. We find that our calculated results are very much comparable with these experimentally based data. Since the TBTE classical cell model of Wasserman *et al* [17] and the present MFP approach share the same source, namely the well-known free-volume theory [30], we also plot the calculated results (as the dashed curve) of Wasserman *et al* in figure 11 for comparison.

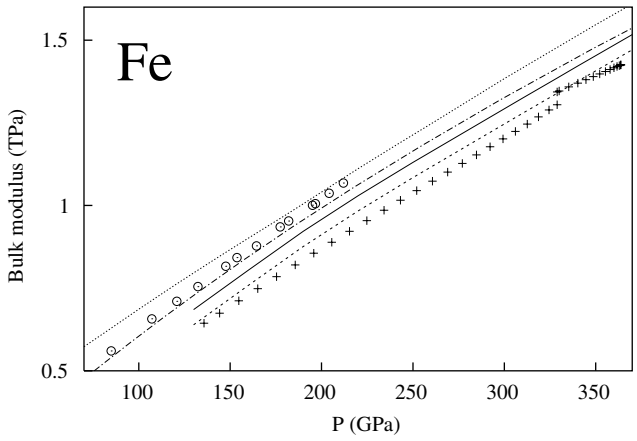

Figure 12. Bulk moduli of hcp Fe. Dotted curve: the first-principles 300 K isothermal values; dot–dashed curve: the deduced 300 K isothermal values from our shock-reduced isotherm; solid curve: the calculated isentropic values under the core conditions obtained by the MFP approach; dashed curve: the isentropic value under the core conditions corrected by considering the shift of our MFP calculation relative to our shock-wave reduction; open circles: the recently measured room temperature values of Mao *et al* [6]; plus signs: the PREM data [24].

6.5. Bulk moduli under the Earth's core pressure

Finally, we depict our calculated bulk moduli in figure 12. Four sets of theoretical values are shown, i.e. set A: the first-principles 300 K isothermal values; set B: the deduced 300 K isothermal values from our shock-reduced isotherm; set C: the calculated isentropic values under the core conditions obtained by the MFP approach; and set D: the version of set C corrected by considering the shift of our MFP calculation relative to our shock-wave reduction. Note that the data of set B are just uniformly smaller, by $\sim$20 GPa (note the value of the bulk moduli being $\sim$1000 GPa), than the recently measured values of Mao *et al* [6], and the data of set D exactly constitute the upper bound of the PREM data.

7. Conclusion

We have performed an *ab initio* thermodynamic calculation for iron. We presented the calculated 300 K static EOS at pressures up to 1000 GPa and the calculated Hugoniot state at pressures and temperatures up to 1000 GPa and 30 000 K, studied the shock-wave data reduction, and reported the calculated thermodynamic properties under the conditions of the Earth's core. The present work is unique in that all the thermodynamic quantities are derived from only 0 K data derived from the accurate LAPW calculation. The present calculation is parameter free in that we do not use the Debye temperature, nor the Grüneisen parameter. In an application to iron, the present study demonstrates again the higher accuracy and greater applicability of the MFP approach [25, 26].

Acknowledgments

This work was supported by the Chinese National PAN-DENG Project (grant no 95-YU-41), the Swedish Foundation for Strategic Research (SSF), the Swedish Natural Science Research Council (NFR), and the Göran Gustafsson Foundation.

References

[1] Huang E, Bassett W A and Tao P 1987 *J. Geophys. Res.* **92** 8129
[2] Jephcoat A P, Mao H K and Bell P M 1986 *J. Geophys. Res.* **91** 4677
[3] Mao H K, Wu Y, Chen L C and Shu J F 1990 *J. Geophys. Res.* **95** 21 737
[4] Merkel S, Goncharov A F, Mao H K, Gillet P and Hemley R J 2000 *Science* **288** 1626
[5] Dubrovinsky L S, Saxena S K, Tutti F, Rekhi S and LeBehan T 2000 *Phys. Rev. Lett.* **84** 1720
[6] Mao H K, Shu J, Shen G, Hemley R J, Li B and Singh A K 1998 *Nature* **396** 741
[7] Barker L M and Hollenbach R E 1974 *J. Appl. Phys.* **45** 4872
[8] Marsh S P 1980 *Los Alamos Shock Hugoniot Data* (Berkeley, CA: University of California Press)
[9] Brown J M and McQueen R G 1986 *J. Geophys. Res.* **91** 7485
[10] Hixson R S and Fritz J N 1992 *Shock Compression of Condensed Matter—1991* ed S C Schmidt, R D Dick, J W Forbes and D G Tasker (Amsterdam: Elsevier) p 69
[11] Brown J M, Fritz J N and Hixson R S 2000 *J. Appl. Phys.* **88** 5496
[12] Anderson W W and Ahrens T J 1994 *J. Geophys. Res.* **99** 4273
[13] Yoo C S, Holmes N C, Ross M, Webb D J and Pike C 1993 *Phys. Rev. Lett.* **70** 3931
[14] Ahrens T J, Holland K G and Chen G Q 1998 *Shock Compression of Condensed Matter—1997* ed S C Schmidt, D P Dandekar and J W Forbes (New York: American Institute of Physics) p 133
[15] Goffaux C, Sánchez-Dehesa J, Yeyati A L, Lambin Ph, Khelif A, Vasseur J O and Djafari-Rouhani B 2002 *Phys. Rev. Lett.* **88** 235502
[16] Stixrude L, Cohen R E and Singh D J 1994 *Phys. Rev.* B **50** 6442
[17] Wasserman E, Stixrude L and Cohen R E 1996 *Phys. Rev.* B **53** 8296
[18] Herper H C, Hoffmann E and Entel P 1999 *Phys. Rev.* B **60** 3839
[19] Söderlind P, Moriarty J A and Wills J M 1996 *Phys. Rev.* B **53** 14 063
[20] Alfè D, Kresse G and Gillan M J 2000 *Phys. Rev.* B **61** 132
[21] Alfè D, Price G D and Gillan M J 2001 *Phys. Rev.* B **64** 045123
[22] Laio A, Bernard S, Chiarotti G L, Scandolo S and Tosatti E 2000 *Science* **287** 1027
[23] Belonoshko A B, Ahuja R and Johansson B 2000 *Phys. Rev. Lett.* **84** 3638
[24] Dziewonski A M and Anderson D L 1981 *Phys. Earth Planet. Inter.* **25** 297
[25] Wang Y 2000 *Phys. Rev.* B **61** 11 863
[26] Wang Y, Chen D and Zhang X 2000 *Phys. Rev. Lett.* **84** 3220
[27] Blaha P, Schwarz K and Luitz J 1999 *WIEN97, a Full Potential Linearized Augmented Plane Wave Package for Calculating Crystal Properties* Technical University of Vienna (ISBN 3-9501031-0-4)
This is an improved and updated Unix version of the original copyrighted WIEN code, which was published by Blaha P, Schwarz K, Sorantin P and Trickey S B 1990 *Comput. Phys. Commun.* **59** 399
[28] Dugdale J S and MacDonald D K C 1953 *Phys. Rev.* **89** 832
[29] Wallace D C 1997 *Phys. Rev.* E **56** 1981
[30] Vashchenko V Ya and Zubarev V N 1963 *Sov. Phys.–Solid State* **5** 653
[31] Cohen R E and Gülseren O 2001 *Phys. Rev.* B **63** 224101
[32] Landau L D and Lifshitz E M 1980 *Statistical Physics* (Oxford: Pergamon)
[33] Boness D A and Brown J M 1990 *J. Geophys. Res.* **95** 21 721
[34] Perdew J P, Burke S and Ernzerhof M 1996 *Phys. Rev. Lett.* **77** 3865
[35] Wang F M and Ingalls R 1998 *Phys. Rev.* B **57** 5647
[36] Ross M, Young D A and Grover R 1990 *J. Geophys. Res.* **95** 21 713
[37] McQueen R G, Marsh S P, Taylor J W, Fritz J N and Carter W J 1970 *High-Velocity Impact Phenomena* ed R Kinslow (New York: Academic) p 293
[38] Vinet P, Rose J H, Ferrante J and Smith J R 1989 *J. Phys.: Condens. Matter* **1** 1941
[39] Moriarty J A 1995 *High Pressure Res.* **13** 343
[40] Wang Y, Ahuja R and Johansson B 2002 *Phys. Rev.* B **65** 014104